ap

Asian Journal of Physics
Vol. 28, Nos 10-12 (2019) 1035-1048
Available on: www.asianjournalofphysics.in

Optical metrology via the photorefractive effect

Arun Anand[1] and C S Narayanamurthy[2]

[1]*Applied Physics Department, Faculty of Technology and Engineering, The M S University of Baroda, Kalabhavan P. B. No 51, Vadodara – 390 001, India*

[2]*Department of Physics, Indian Institute of Space Science and Technology(IIST) Valiamala (PO), Thiruvananthapuram 695 547, India*

This article is dedicated to Prof Kehar Singh for his significant contributions to Optics and Photonics

By exploiting the two wave mixing phenomena in crystals of sillienite family like $Bi_{12}SiO_{20}$ (Bismuth Silicon Oxide) and $Bi_{12}TiO_{20}$ (Bismuth Titanium Oxide) optical metrological applications like stress and strain measurements and testing of optical elements can be carried out. In this paper, we report physics of two wave mixing phenomena in photorefractive crystals of sillienite family like BSO, BTO and their applications to optical metrology in detail.

Keywords: Photorefractive effect, Two wave mixing, Dynamic holography, Optical metrology

1 Introduction

Photorefractive crystals are widely used nonlinear optical materials for recording real-time holograms, two wave mixing experiments for image amplifications, phase conjugation, opto-electronic correlators etc, with relatively low intensity requirements [1-6]. This is because of their unlimited recyclability as, they can be recorded and erased with sufficiently high sensitivity. Among the different types of photorefractive crystals which, are widely used for real-time holography and two wave mixing experiments are the crystals of sillienite family like, Bismuth Germanium Oxide ($Bi_{12}GeO_{20}$ or BGO), bismuth silicon oxide ($Bi_{12}SiO_{20}$ or BSO), Bismuth Titanium Oxide ($Bi_{12}TiO_{20}$ or BTO) and polar crystals like Barium Titanate ($BaTiO_3$) and Lithium Niobate ($LiNbO_3$). These crystals possess high sensitivity for volume holographic grating formation [7] that enables them to record holograms in the visual region of the spectrum with continuous wave lasers like He-Ne, He-Cd, Argon Ion etc. Also, these crystals are available in large sizes and good quality. There were many innovative geometries have been proposed by various authors to record holograms in these crystals with and without externally applied electric field across the crystal in both two and four wave mixing geometries [8-14], respectively. Normally two wave mixing geometry similar to conventional holographic geometry with photorefractive crystals as recording medium is used for recording dynamic holograms. Kamshalin *et al* [15], in a simple two wave mixing geometry by exploiting the anisotropic self diffraction phenomena in Bismuth Titanium Oxide ($Bi_{12}TiO_{20}$) stored dynamic hologram and later the same was implemented using Bismuth Silicon Oxide ($Bi_{12}SiO_{20}$) with higher diffraction efficiency by Troth and Dainty [16]. These two dynamic holograms had good efficiency without applied electric field and the main advantage was one can use polarizer and analyzer pair to separate out diffracted beams. This is because in an isotropic self diffraction geometry, the polarization of writing beams (Object and Reference) after interacting inside the crystal gets rotated with respect to direct beams. This enables one to introduce an analyzer after the crystal

Corresponding author :
e-mail: naamu.s@gmail.com (Chittur Subramanian Narayanamurthy)

for separating out the diffracted beams. In fact this, two wave mixing and anisotropic diffraction geometry was very suitable to dynamic holographic interferometry for metrological applications. Also, photorefractive crystals are extensively used for joint optical correlators, coherent enhancements, soliton generations etc [12,13]. But main problem especially for applications to holography remains in terms of non-availability of good quality large size photorefractive crystals. In this paper, we start with in section 2, a detailed explanation about photorefractive effect and then in section 3, about photorefractive dynamic holography applied to photoelasticity using $Bi_{12}SiO_{20}$ (bismuth silicon oxide) and Farady optical rotation measurements using optical activity of $Bi_{12}TiO_{20}$ (bismuth titanium oxide), respectively. These two applications show clearly, the use of photorefractive crystals of silienite like BSO/BTO for real-time dynamic metrology.

2 Theoretical explanation of photorefractive effect

2.1 Introduction

Unlike conventional non-linear optical effects (Phase conjugation, Brillouin scattering, second harmonic generation etc), the light intensity induced susceptibility is not used for photorefractive effect only, relative intensity due to an interference pattern inside the crystal is responsible for photorefractive effect.

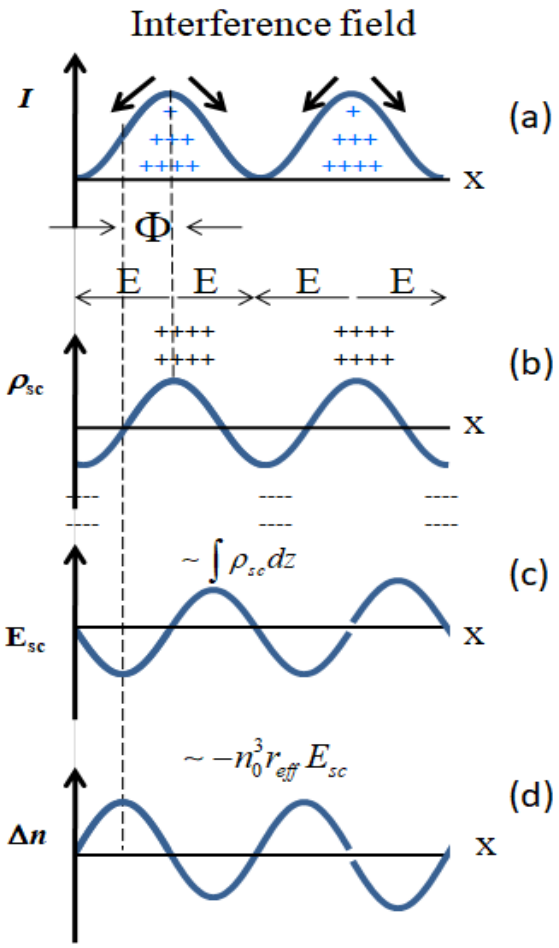

Fig 1. Shows the physics of photorefractive effect.

Figure 1 shows the mechanism of photorefractive effect where, a photorefractive material is illuminated by an interference pattern (In dynamic holography, these would be the signal and reference beams). This interference pattern between the object and reference beams results in a pattern of dark and light fringes throughout the crystal (Fig 1(a)). Now, the charges (either electrons or holes) present, in regions of photorefractive crystal where a bright fringe is present, absorb the light and get photoexcited from an impurity level into the conduction band of the photorefractive crystal, leaving net positive or negative charges. The impurity levels have an energy intermediate between the energies of the valence band and conduction band of the PR crystal and so, the electrons or holes in conduction band of crystal, diffuse throughout the crystal. Since the charges are excited in the region of bright fringes, the net charge diffusion current is towards the dark-fringe regions of the PR crystal and in the conduction band, the charges (electrons and holes), recombine and return to the impurity levels. The rate at which this recombination takes place determines how far the charges (electrons/holes) diffuse, which in turn determines strength of the photorefractive effect in that crystal. Now in the impurity level, the electrons/holes are trapped and can no longer move unless re-excited back into the conduction band by light. This net redistribution of electrons/holes into the dark and bright regions of photorefractive crystal causes space charge field (E_{sc}) in the crystal as shown in Fig 1(c). Since the electrons and holes are trapped and immobile, the space charge field (E_{sc}) remains even after the removal of interference patterns. This internal space charge field (E_{sc}), due to electro-optics effect causes the refractive index of the crystal to change in the regions where the field is strongest and this causes a spatially varying refractive index grating (Dn) shown in Fig 1(d), to occur throughout the crystal.

This dynamic grating can diffract, light shone on to the crystal, and the resulting diffraction pattern recreates the original pattern of light stored in the crystal which is either the object beam/reference beam. Thus a photorefractive crystal can act as dynamic hologram if both object and reference beam interfere in the crystal.

2.2 Theoretical explanation

Consider, $E_1\exp\{i(\vec{k_1}\cdot\vec{r}-\omega t)\}$ is the object beam and $E_2\exp\{i(\vec{k_2}\cdot\vec{r}-\omega t)\}$ the reference beam falling on the photorefractive crystal (Fig 2), then the total intensity I_t incident on the photorefractive crystal will be following Appendix 1 as,

$$I_t = I_0\,[1 + M\cos(k_g x + \varphi)] \tag{1}$$

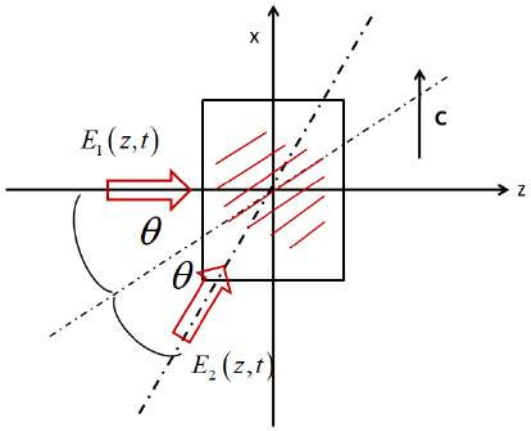

Fig 2. Two beam interference used in the explanation.

where, I_0 and M represent intensity and modulation ratio ($0 \le M \le 1$) as given in Appendix 1. Here, we have assumed that the amplitude of the object and reference beam are different. Now, if N is the concentration of

charges (electrons/holes) in the conduction band then the net generation rate of charges (electrons/holes) G_e will be given by the difference between the rates of generation and recombination of electrons/holes to the donor level, which is equal to,

$$G_e = (\beta_e + sI_t)\,(N_D - N_D^+) - \gamma_e N_D N_D^+ \tag{2}$$

where, s is the photo-ionization coefficient, G_e is the recombination constant, and β_e is the thermal excitation rate of electrons/holes [14]. Also N_D and N_D^+ represent the density of the donors and the density of ionized donors respectively and I_t is the total light intensity incident on the crystal. Generally, the motion of electrons/holes in the conduction band can be attributed to three forces (i) drift force due to external applied field, (ii) due to photovoltaic effect and (iii) diffusion force due to incident spatially modulated light intensity from regions of higher concentration to regions of lower concentration. So, assuming that the electrons move due to above forces, the current in the crystal can be written as following [14],

$$J_e = eN\mu_e E + \mu_e k_B T \frac{\partial n}{\partial x} + p_n (N_D - N_D^+)\, I_t \tag{3}$$

where, N is the number densities of conduction band electrons, μ_e is the electron mobility, p_n is the photovoltaic constant, E is the electric field and e is the electric charge. Combining Eqs (2) and (3) in continuity equations, we can write the variations of the electron/holes concentration with time as,

$$\frac{\partial N}{\partial t} = G_e + \frac{1}{e}\frac{\partial J_e}{\partial x} \tag{4}$$

In a similar way, we can write the continuity equation for density of ionized donors as,

$$\frac{\partial N_D^+}{\partial t} = G_e \tag{5}$$

Then, using Poisson's equation the electric field in the crystal can be written as,

$$\frac{\partial E}{\partial x} = \frac{e}{\varepsilon_s}(N_D^+ - N_A^- - N) \tag{6}$$

where, ε_s is the static dielectric permittivity and is independent of position and N_A^- is the ionized acceptor density. In arriving at Eq (6) we have assumed that the illumination varies only along one dimension. The electrostatic condition implies that

$$\nabla \times \vec{E} = 0 \tag{7}$$

Also assuming that $N << N_A$, $N_D - N_A$, $N_D^+ \approx N_A$), in the steady state, the equation for number of free electron becomes,

$$N = N_0 \left[1 + m\, cos\, (\vec{k_g} \cdot \vec{x})\right] \tag{8}$$

where, $N_0 = g(I_0)\tau$, $g(I_0)$ is the linear generation rate and τ_R is the free electron life time. Here, m is the reduced fringe contrast modulation ratio given by,

$$m = M/(1 + (\beta / sI_0)) \tag{9}$$

Integrating Eq (6), once with respect to x we have the electric field component,

$$E = \frac{\left(J_e - eD\frac{\partial n}{\partial x}\right)}{e\mu_e N} \tag{10}$$

where D is the diffusion coefficient, $D = m_e k_B T/e$

Substituting the respective values for current, number of free electrons etc and simplifying, Eq (10) reduces to,

$$E = \frac{J_e}{e\mu_e N_0}\cdot\frac{1}{1 + m\,\cos\,(k_g x)} - \frac{Dk_g}{\mu_e}\cdot\frac{m\,\sin(k_g x)}{1 + m\,\cos(k_g x)} \tag{11}$$

If, the applied voltage is V over a material of length L then Eq (11) changes to

$$\frac{1}{L}\int_0^L E\,dx = \frac{V}{L} = \frac{J_e}{e\mu_e N_0}\frac{1}{L}\int_0^L \frac{1}{1+m\cos(k_g x)}\,dx - \frac{Dk_g}{\mu_e}\frac{1}{L}\int_0^L \frac{m\sin(k_g x)}{1+m\cos(k_g x)}\,dx \tag{12}$$

For integral number of very large numbers of fringes in L,

$$\frac{1}{L}\int_0^L \frac{1}{1+m\cos(k_g x)}\,dx = \frac{1}{\sqrt{1-m^2}}$$

$$\frac{1}{L}\int_0^L \frac{m\sin(k_g x)}{1+m\cos(k_g x)}\,dx = 0 \tag{13}$$

which implies,

$$J_e = (1-m^2)^{1/2}\,\sigma_0\,E_A \qquad \text{and} \qquad \sigma_0 = e\mu_e N_0 \tag{14}$$

where $E_A = V/L$ is the applied electric field [14].

It may be noted that for the applied electric field, the conductivity of cosinusoidal illumination is reduced by a factor $\sqrt{1-m^2}$ related to the conductivity at the same average intensity [14]. Rewriting, Eq (11) and after simplification using little algebra, we get

$$E = E_A\cdot\frac{\sqrt{1-m^2}}{1+m\cos(k_g x)} - E_D\cdot\frac{m\sin(k_g x)}{1+m\cos(k_g x)} \tag{15}$$

In Eq (15), E_D is called as the characteristic field,

$$E_D = \frac{D\,k_g}{\mu_e} = \left(\frac{K_B\,T}{e}\right)k_g \tag{16}$$

where, T is the room temperature and K_B is the Boltzmann constant. The characteristic field is independent of the material and it depends only on the temperature. If an external electric field is not applied, then charge migration is due to diffusion alone and Eq (15) reduces to,

$$E_{sc} = -E_D\frac{m\sin(k_g x)}{1+m\cos(k_g x)} \tag{17}$$

The Eq (15) is the space charge field (for diffusion alone) and is denoted by E_{sc}. In photorefractive materials this space charge field plays an important role and is created by two different mechanisms using drift (with the applied field) and diffusion (without applied field). The space charge field which, is created due to charge separation will introduce a change in the index of refraction via the linear electro-optic effect (Pockel's effect) and is given by [12,13]

$$\Delta n = \frac{1}{2}n_r^3\,r_{\text{eff}}E_{sc} \tag{18}$$

where Δn is the change in refractive index, r_{eff} is the effective electro-optic coefficient and n_r is the unperturbed refractive index. This change in the index of refraction will lead to a refractive index grating and the diffraction efficiency (η) of such grating is given by [12],

$$\eta = \exp-\left(\frac{\alpha t}{\cos\theta_B}\right)\sin^2\left(\frac{\pi t}{\lambda\cos\theta_B}\Delta n\right) \tag{19}$$

where, α is the absorption co-efficient of the crystal, t is the thickness of the crystal, λ is the wavelength of incident light and θ_B is the Bragg's angle inside the crystal. Since, in photorefractive holography both writing and reading holograms are done simultaneously in real-time, the light will diffract from this refractive index

grating after mixing. Therefore, there can be transfer of energy from reference (probe) beam to the object (signal) beam. The efficiency of dynamic holograms recorded in the photorefractive crystals depends upon this energy transfer and is known as the photorefractive gain Γ which, can be written as following [12],

$$\Gamma = \frac{2\pi}{\lambda} n_r^3 r_{\text{eff}} E_{SC} \tag{20}$$

where, λ is the wavelength of light used.

3 Optical metrology using photorefractive crystals

In this section, we describe two applications of photorefractive crystals of sillienite family namely $Bi_{12}SiO_{20}$ (bismuth silicon oxide) and $Bi_{12}TiO_{20}$ (bismuth titanium oxide) for dynamic (real-time) photoelasticity and for measuring weak Faraday optic rotation, respectively. These two works have been reported earlier separately [25,28] and we give some part of results to establish the use of BSO/BTO for metrological applications. Section 3.1 describes real-time holographic photoelatsicity using $Bi_{12}SiO_{20}$ and section 3.2 describes measurement of weak Faraday optical rotation using $Bi_{12}TiO_{20}$.

3.1 Real-time holographic photoelasticity using $Bi_{12}SiO_{20}$ (bismuth silicon oxide)

3.1.1 Introduction

Photoelasticity is an experimental stress analysis technique in which the state of stress in certain transparent non-crystalline materials is determined by its effect on the polarization state of light, when trans-illuminated through them with a polarized light [17-21]. Such materials are widely used in launch vehicles, space crafts and in many machines and equipments. These transparent non-crystalline materials can be divided in to two categories, namely birefringent (refractive index dependent due to application of stress) and non-birefringent (non-dependent of refractive index due to applied stress) materials, respectively. Normally, birefringent, materials are isotropic when there is no applied stress and becomes an-isotropic (birefringent), whenever stress is applied. The refractive indices of stress induced birefringent materials become n_1 and n_2 along the directions of the principal stresses σ_1, σ_2, respectively whenever a polarized light beam passes through it. Such stress induced birefringent material when viewed, through crossed polarizers, exhibits two types of fringe systems, namely isochromatic and isopachic. The fringe system which separates the difference in principal stresses is known as isochromatic and they are contours of constant values of ($\sigma_1 - \sigma_2$) and which adds principal stresses are called isopachic and they are contours of constant values of ($\sigma_1 + \sigma_2$), respectively [17]. Photoelasticity actually can map the differences in principal stresses ($\sigma_1 - \sigma_2$) and addition of principal stresses ($\sigma_1 + \sigma_2$) in birefringent materials under stress, making use of *Maxwell-Neumann* equations. Numerous classical optical methods like, polarimeter, *Mach-Zehnder* interferometer, conventional holographic interferometer have been widely used to find the isochromatic and isopachic fringes of stress induced birefringent materials [17-21]. Compared with classical optical interferometric techniques, like polariscopes and Mach-Zehnder Interferometer, the holographic technique introduced by Fourney and Mate and Hovenesian *et al* [20,21] to find simultaneously the sum (isopachic) and difference (isochromatic) fringes alleviated most of the problems associated with the classical interferometric techniques. But, the problem of wet processing of recorded holograms still posed problems and also the analysis of phase information from the recorded hologram. To solve this, a new technique based on dynamic (Real-Time) holography using photorefractive effect in BSO is proposed.

3.1.2 Experimental procedure and theory

Figure 3 shows the typical experimental geometry used for recording dynamic holographic photoelasticity using photorefractive BSO (bismuth silicon oxide). The test specimen (A plastic ruler made up of photoelastic material) is illuminated by a diffuse illumination via the Diffuser (Fig 3) and is imaged on to a BSO sandwiched between two polarizers with $1/4^{\text{th}}$ magnification. This is required for imaging on to a TV monitor via CCD (Charge Coupled Devise camera). A reference beam from same laser which illuminated

the diffuser is allowed to fall on the crystal as shown in Fig 3. The object beam from test specimen and reference beam interfere in the BSO crystal and dynamic hologram of test specimen is formed. Since the crystal exhibits a strong an-isotropic self diffraction, the dynamic hologram of test specimen can be separated out from direct diffracted beam by rotating the analyzer after the crystal.

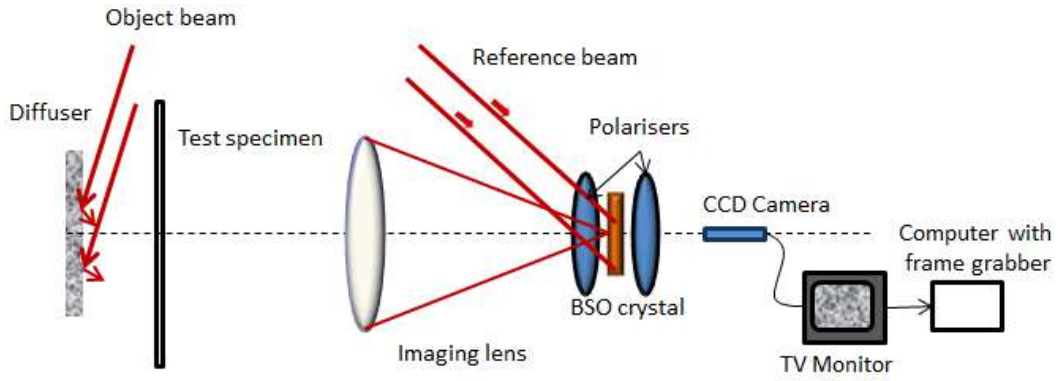

Fig 3. Experimental geometry for dynamic holographic photoelasticity using BSO.

Here, the procedure to be followed is a double exposure dynamic holography that is first dynamic hologram is taken when the object is under no stress and the second dynamic hologram is taken after the stress is given to the test specimen. Consider, $E_{01}\exp(-if_1)$, $E_{02}\exp(-if_2)$,(virtual and real), represent reconstructed waves of holograms before stress and $E'_{01}\exp(-i(f_1+\Delta f_1)$, $E'_{02}\exp(-i(f_2+\Delta f_2)$ represent the second reconstructed holograms (virtual and real) after stress is given to the photoelastic specimen inside the BSO crystal. In that Δf_1 and Δf_2 are the phase changes due to stressing the object. Now the intensity of photorefractive dynamic hologram inside the crystal which is captured by CCD and following Vest [17], is given by,

$$I_T = \left|2E_{01} + E'_{01} + E'_{02}\right|^2 \tag{21}$$

Since, before applying stress the light beam passing through the object is isotropic the amplitude and phase of light waves are assumed to be equal as ($E_{o1}\, e^{-i\phi 1} = E_{o2}\, e^{-i\phi 2}$) and that is why the first term in Eq (21) is $2E_{o1}$. Evaluating the terms inside the bar further, by multiplying with its complex conjugate the irradiance of reconstructed wave will be proportional to,

$$I_H = 2\left[1+\cos\left(\frac{\Delta\phi_1+\Delta\phi_2}{2}\right)\cos\left(\frac{\Delta\phi_1-\Delta\phi_2}{2}\right)+\cos^2\left(\frac{\Delta\phi_1-\Delta\phi_2}{2}\right)\right] \tag{22}$$

For stress birefringent objects like the photoelastic specimen, using Maxwell-Neumann's law we get,

$$\Delta\phi_1 - \Delta\phi_2 = \frac{2\pi}{\lambda}\, t'\,[(A-B)\,(\sigma_1-\sigma_2)] \tag{23}$$

$$\Delta\phi_1 + \Delta\phi_2 = \frac{2\pi}{\lambda}\, t'\,[(A+B) - 2\frac{\nu}{E}\,(n_1-n_2)]\,(\sigma_1+\sigma_2) \tag{24}$$

where, ν is the *Poisson's* ratio, E is the modulus of elasticity of the test specimen and t' is the thickness of the specimen. Simplifying further by substituting Eqs (23) and (24) in Eq (22), we get the irradiance value proportional to,

$$I = 1 + 2\cos\left[\frac{\pi t_o}{\lambda}(A'+B')(\sigma_1+\sigma_2)\right]\cdot\cos\left[\frac{\pi t_o}{\lambda}\,C(\sigma_1-\sigma_2)\right]+\cos^2\left[\frac{\pi t_o}{\lambda}C(\sigma_1-\sigma_2)\right] \tag{25}$$

where,

$$A' = A - \frac{v}{E}[(n_1 - n_2)]$$

$$B' = B - \frac{v}{E}[(n_1 - n_2)]$$

$$C = A - B$$

Equation (25) represents final intensity of dynamic hologram recorded in photorefractive BSO where, the third term in the intensity equation represents classical isochromatic ($\sigma_1 - \sigma_2$) fringe pattern, but it is not directly separated from combined isopachic ($\sigma_1 + \sigma_2$) and isochromatic terms represented by the first two terms in the intensity equation. Thus it is impossible to separately obtain pure isochromatic ($\sigma_1 - \sigma_2$) fringes and only hologram of a stressed specimen can give a combination of both isochromatic and isopachic fringes superposed with isoclinic fringes [17]. Experiments were carried out using a stressed specimen (plastic ruler, mainly available along with school geometry box) and an unstressed specimen made up of polymetylmetacrylate (PMMA) of thickness of 6 mm. An 1 Watt Argon-ion gas laser was used as source along with a 110 cut, Bi_{12} SiO_{20} (bismuth silicon oxide) crystal size of 10 mm ×10 mm × 10mm sandwiched between two polarizers as recording photorefractive crystal.

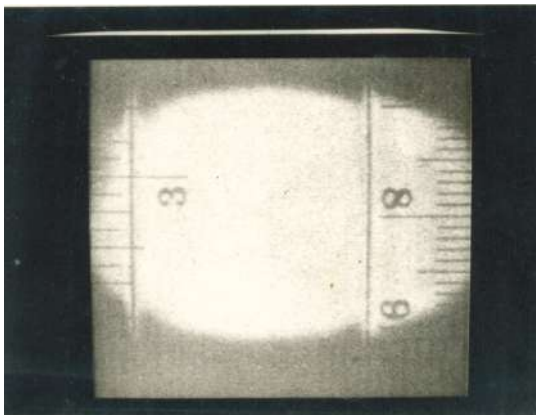

Fig 4(a). Dynamic hologram of a plastic ruler made up of photoelastic PMMA

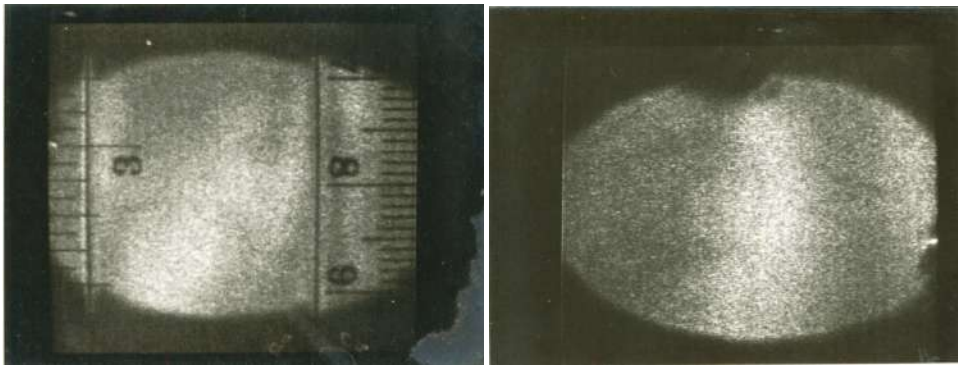

Fig 4 (b). Isochromatic Fringe system Fig 4(c). Isopachic Fringe system

Figure 4(a) shows the dynamic hologram recorded inside photorefractive BSO of a stressed photoealstic specimen (plastic ruler) when illuminated by a diffuse beam from diffuser and (4b) and (4c) show

the isochromatic ($\sigma_1 - \sigma_2$) and isopachic ($\sigma_1 + \sigma_2$) fringe systems of same dynamic hologram, respectively. The method is real-time [24] and as soon as laser beam is on one can directly obtain the dynamic hologram on the monitor of PC connected to the CCD/CMOS camera.

3.2 Faraday Rotation measurement using $Bi_{12}TiO_{20}$ (bismuth titanium oxide)

3.2.1 Introduction

Faraday optical effect is the rotation of plane of vibration of linearly polarized light passing through a material medium due to applied magnetic field [26,27]. The Faraday optical effect is used in a number of applications like analysis of mixture of hydrocarbons, modulators, etc. [27]. But, most of the materials showing Faraday effect have very small rotations as the applied magnetic fields are small making it difficult to measure. For example, rotation produced by a 1 cm column of H_2O in an applied magnetic field of 10^4 Gauss is only 2°11'. So using Malu's law [27] and conventional detectors like photodiodes it is difficult to measure this small rotation very accurately. So, it becomes essential to enhance such feeble rotation. Optical activity is the rotation of plane of polarization of linearly polarized light passing through optically active materials [26]. Some of the popular materials, which exhibit strong optical activity, are the photorefractive materials of silliniete family namely BSO, BGO and BTO [12,13].

3.2.2 Experimental procedure and Results

Since photorefractive $Bi_{12}TiO_{20}$ (bismuth titanium oxide) responds very efficiently to low power He-Ne lasers at 633 nm, and exhibits strong optical activity, we use the same to enhance weak Faraday-Optic rotation in the experimental geometry shown in Fig 5.

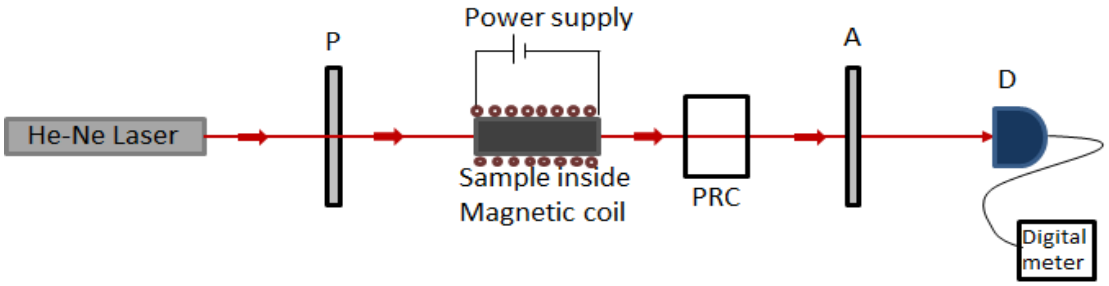

Fig 5. Shows the experimental geometry for measuring weak Faraday Optic rotation.

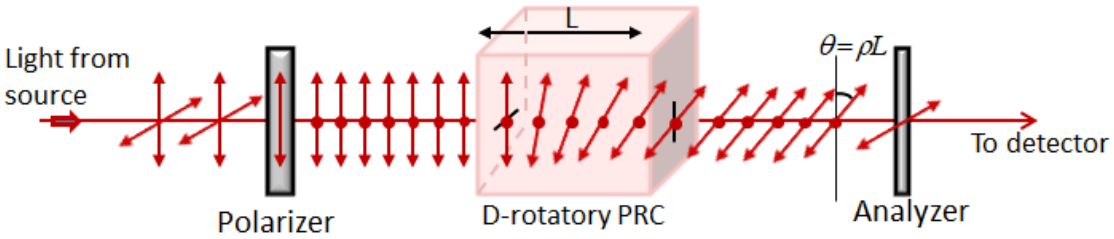

Fig 6. Shows the optical activity of photorefractive crystal.

The experimental setup used in this method is given in Fig 5 where the light, from a He-Ne laser source of 20mW at 632.8 nm passes through a linear polarizer P. This linearly polarized light then passes through the sample S (Quartz) whose magneto-optic rotation was to be measured. The sample was kept inside a magnetic coil. The light after passing through the sample falls on the photorefractive $Bi_{12}TiO_{20}$ (PRC), which then passes through the analyzer A to the detector D. Before putting the photorefractive crystal the analyzer–polarizer pair was crossed so that the detector output was made to zero. The photorefractive

$Bi_{12}TiO_{20}$ was then introduced in the setup and the output was measured without applied magnetic field. The photorefractive crystal used was a d-rotatory $Bi_{12}TiO_{20}$ of 5 mm thickness with [1 1 0] cut. The detector showed measurable output due to the optical activity of the photorefractive crystal [28]. Whenever, the linearly polarized light passes through the photorefractive BTO, it is decomposed into its constituents (left and right circularly polarized), which travel through the medium with different velocities. This will result in a phase difference of ψ between the two waves. After coming out from the crystal these waves will recombine to form a linearly polarized light with its plane of polarization rotated by and angle equal to ψ/2 making the linearly polarized light no longer crossed with the analyzer resulting in a change in the output (Fig 6).

The amount of rotation of the plane of polarization is decided by the specific rotation (ρ) and the thickness of the crystal (L) and is given by [27]

$$\theta = \rho L. \tag{1}$$

The specific rotation ρ is given by [27]

$$\rho = (n- - n+)/\,l \tag{2}$$

where $n-$ and $n+$ are the refractive indices for left and right circularly polarized waves, respectively, and l is the wavelength of light used. Depending on the values of n− and n+ the output will be either d-rotatory or l-rotatory [26,27]. Initially the light output from the crystal output, without applying the magnetic field will give the rotation due to optical activity of the photorefractive $Bi_{12}TiO_{20}$ alone and when the magnetic field B is switched on and increased gradually the detector outputs will show the increased value. The angle ϕ through which the plane of vibration rotates is given by [26,27]

$$\phi = V\,d; \tag{3}$$

where B is the static magnetic flux density in gauss, d is the length of medium traversed in cm and V is the proportionality constant called Verdet constant, respectively. A positive Verdet constant corresponds to a material for which Faraday effect is l-rotatory when the light moves parallel to the applied field and d-rotatory when it propagates anti-parallel to applied magnetic field B. The samples used in the experiments had positive Verdet constants. The sample used in the experiments was quartz (V = 0:0166 G=cmat 20◦C) samples [26]. The magnetic field was first applied in such a direction that it is anti-parallel to the direction of propagation of light and this will rotate the plane of polarization clockwise (d-rotatory). Since the PR crystal used here, that is, $Bi_{12}TiO_{20}$ is purely d-rotatory, the light after passing through it will produce an increased output, which is more than that due to $Bi_{12}TiO_{20}$ alone (Fig 7). This increase is measured for further analysis. Now the direction of magnetic field was reversed and the same procedure was repeated. Now the plane of polarization is rotated anti-clockwise (l-rotatory) making the output less than that due to $Bi_{12}TiO_{20}$ alone (Fig 8). The total angle of rotation either Θ = (θ + ϕ) or Θ = (θ − ϕ) can be calculated from Malu's law [26]

$$I = I_0 \cos^2\Theta \tag{4}$$

where I is the detector output and I_0 is the output without the analyzer which is a constant for a particular source power. The positive (+) sign is when the magnetic field B was applied anti-parallel to light propagation and the sample is d-rotatory resulting in an increased rotation of plane of polarization as the d-rotation of the sample enhances the d-rotation by the photorefractive crystal (Fig 7).

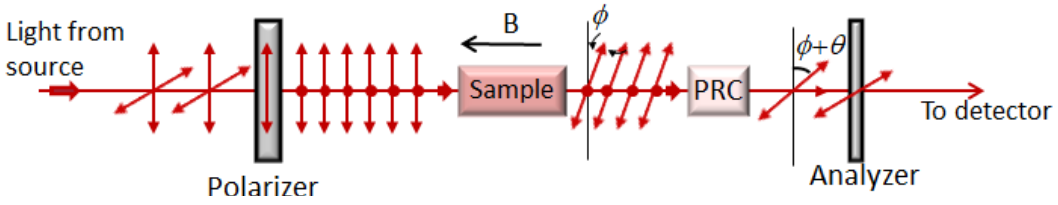

Fig 7. Total optical rotation with B anti-parallel to light propagation (d-rotation).

The negative (−) sign is when the applied magnetic field B is parallel to light propagation and the sample is l-rotatory resulting in a decreased rotation of plane of polarization as the l-rotation of the sample combines destructively with the d-rotation by the photorefractive crystal (Fig 8). By using the value of ρ the magneto-optic rotation ϕ of the sample can be calculated.

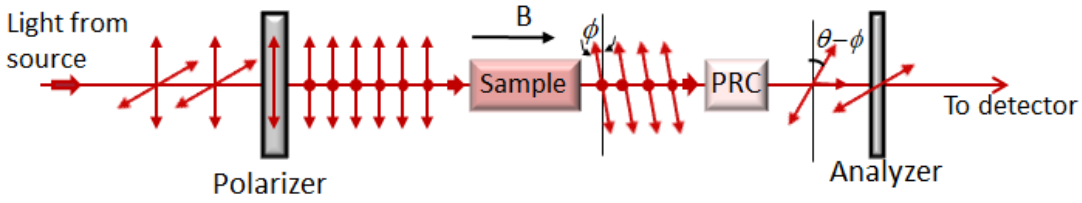

Fig 8. Total optical rotation with B parallel to light propagation (l-rotation)

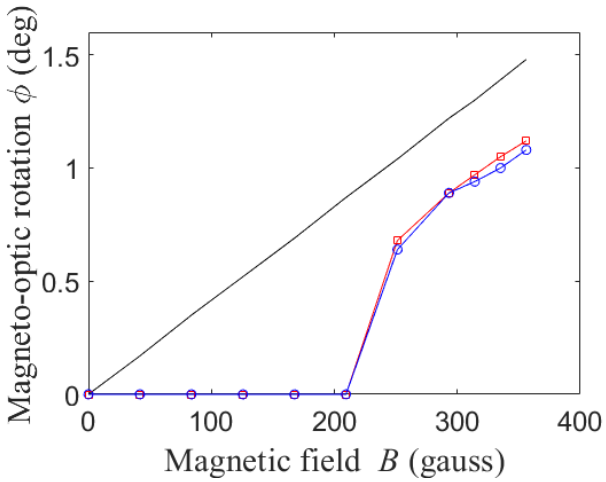

Fig 9. Change in magneto-optic rotation with applied field for direct measurement for a sample 1ength equal to 15 cm with source power of 20 mW.

The experiments were carried out with two different source intensities of 20 and 8 mW, respectively and with two experimental samples of different lengths (Sample 1 with 15 cm and Sample 2 with 5 cm). The magnetic field was varied from 0 to 360 Gauss and corresponding output intensities are measured using commercially available detectors and digital meters. The samples were kept inside a coil having turns 250 turns/cm and along the propagation path of the beam. First, output from the sample was first measured without the photorefractive crystal along the path of the beam with the polarizer–analyzer pair kept at crossed position for both the magnetic field (B), applied parallel and anti-parallel to light propagation, respectively. From this, the Faraday rotation due to the experimental sample was found out using Malu's law ($I = I_0 \cos^2\Theta$). Initially, for the 15 cm sample the detector did not measure any change in the output until the magnetic field was increased to 250 Gauss which is shown in Fig 9. Also, whenever the source intensity was reduced from the maximum output, it became still more difficult to measure. Only when the magnetic field was increased to 290 Gauss, the detector showed any measurable output. On the other hand, for the 5 cm sample the detector output did not show any output intensity values, even for an applied magnetic field of 500 Gauss, and with 20 mW source intensity. At this stage, the photorefractive $Bi_{12}TiO_{20}$ was introduced and kept after the sample as shown in Fig 7. This instantly increased the output in the detector, indicating high optical rotation. Measurements were taken again for the magnetic field direction, along parallel and anti-parallel directions to light propagation. As explained earlier when magnetic field (B) was applied anti-parallel to

direction of propagation of light the rotation was more than the optical rotation due to $Bi_{12}TiO_{20}$ alone and when magnetic field (B) was applied parallel to direction of propagation the rotation was less than the optical rotation due to $Bi_{12}TiO_{20}$ alone.

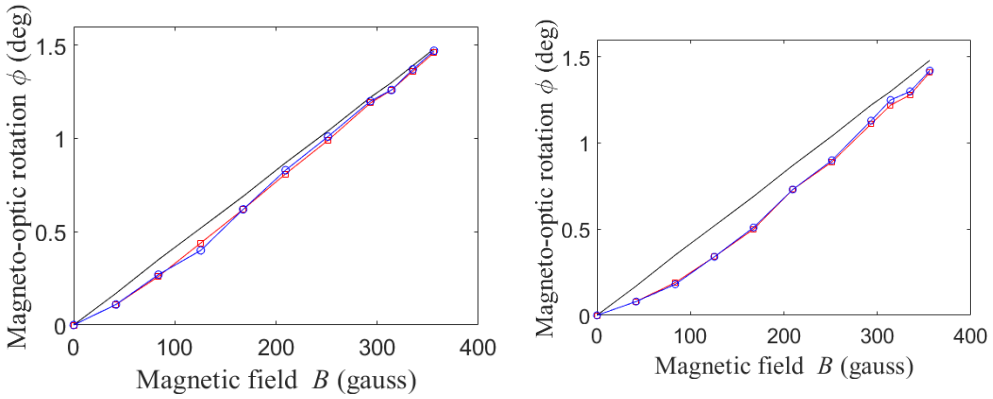

Fig 10. (a) Change in magneto-optic rotation with applied 5eld with photorefractive $Bi_{12}TiO_{20}$ for Sample 1 (15 cm) with source power of 20 mW. (b) Change in magneto-optic rotation with applied field with photorefractive $Bi_{12}TiO_{20}$ for Sample 2 (5 cm) with source power of 20 mW.

The plots of these changes in magneto-optic rotation with the applied magnetic field are shown in Figs 10 (a), and (b), respectively. These plots clearly show that the experimentally obtained (squares) values match very well with the theoretically (circles) predicted values. From these plots, it can be clearly seen that the proposed method gives very accurate results even for small magnetic fields, whereas the direct measurement for small magnetic fields deviate grossly from theoretically predicted values. The experimentally obtained values become closer to the theoretically predicted values when the magnetic field is increased.

4 Conclusion

The paper starts with introduction to photorefractive optics and then in section 2, a detailed explanation about physics of photorefractive effect was given. Further, to demonstrate the capability of photorefractive crystals for metrological applications, we have demonstrated two experiments one using photorefractive $Bi_{12}SiO_{20}$ (Bismuth silicon oxide) for finding photoelastic stress and strains of birefringent samples in terms of isochromatic and isopachic fringe system via dynamic holography and the second one for measuring weak Faraday optical rotation using photorefractive $Bi_{12}TiO_{20}$ (bismuth titanium oxide), respectively. These two experiments clearly show the application of BSO and BTO for optical metrology.

5 Acknowledgement

The authors wish to thank *Prof R S Sirohi* for giving this opportunity to write this article in honor of *Prof Kehar Singh*, who has worked extensively using photorefractive crystals especially using $BaTiO_3$(barium titanate). One of the authors (CSN) acknowledges DST(Govt of India) for awarding the BOYSCAST fellowship during 1991-92 to work at Imperial College, London, UK for carrying out part of the work reported in this paper. The authors gratefully acknowledge *Department of Science and Technology* (DST) Govt of India and University Grants Commission (UGC), New Delhi for providing the financial assistance through their respective project grants (SP/S2/L-15/94) and F-10-7/2001(SR-1) to carry out part of this work at Applied Physics Department, Faculty of Technology and Engineering, The M S University of Baroda, Vadodara.

References

1. Gower M, Dynamic holograms from crystals, *Nature*, 316(1985)12-14.
2. Yariv A, Yeh P, Optical waves in crystals, Chap 13, (Wiley), 1984.
3. Laeri F, Tschudi T, Albers J, Coherent cw image amplifier and oscillator using two wave interaction in a $BaTiO_3$-crystal, *Opt Commun*, 47(1983)387-390.
4. Plastis D, Yu J, Hong J, Bias free time integrating optical correlator using a photorefracive crystal, *Appl Opt*, 24 (1985)3860-386.
5. Huignard J P, Marrakchi A, Coherent signal beam amplification in two wave mixing experiments with $Bi_{12}SiO_{20}$ crystals, *Opt Commun*, 38(1981)249-254.
6. Rajenbach H, Bann S, Refregier P, Joffre P, Huignard J P, Buchkremer H S, Jensen A S, Rasmussen E, Brenner K H, Lohmann G, Compact photorefractive correlator for Robotic applications, *Appl Opt*, 31(1992)5666-5674.
7. Huignard J P, Herriau J P, Valentin T, Time-Average holographic interferometry with photoconductive electro-optic $Bi_{12}SiO_{20}$ crystals, *App Opt*, 16(1977)2796-2798.
8. Huignard J P, Herriau J P, Aubourg P, Spitz E, Phase conjugate wavefront generation via real-time holography in $Bi_{12}SiO_{20}$ crystals, *Opt Lett*, 4(1979)21-23.
9. Stepanov S I, M P Petrov M P, Efficient unstationary holographic recordings in photorefractive crystals under external alternating electric fields, *Opt Commun*, 53(1985)292-295.
10. Tschudi T, Herden A, Goltz J, Klumb H, Laeri F, Albers J, Image amplification by two wave and four wave mixing in $BaTiO_3$ photorefractive crystals, *IEE J Quantum Electron*, 22(1986)1493-1502.
11. Yeh P, Introduction to photorefractive nonlinear optics, (John Wiley & Sons Inc, New York), 1993.
12. Solimar L, Webb D J, Grunnet-Jepsen A, The physics and applications of photorefractive materials, Oxford series in optical imaging and sciences, (Clarendon Press, Oxford), 1996.
13. Stepanov S I, Petrov M P, Nonstationary holographic recording for efficient amplification and phase conjugation in: Photorefractive Materials and Applications I, Topics Appl Phys, (eds) Gunter P, Huignard J P, Vol 61, (Springer, Berlin, Heidelberg), 1988.
14. Hall T J, Jaura R, Connors L M, Foote P D, The photorefractive effect : A review, *Prog Quantum Electron*, 10(1985)77-144.
15. Kamshilin A A, Mokrushina E V, Petrov M P, Adaptive holographic interferometers operating through self-diffraction of recording beams in photorefractive crystals, *Opt Eng*, 28(1989)580-588.
16. Troth R C, Dainty J C, " Holographic interferometry using an-isotropic self diffraction in $Bi_{12}SiO_{20}$, *Opt Lett*, 16(1991)53-55.
17. Vest C M, Holographic interferometry, (John Willey & Sons: New York), Chapter 7, 1971.
18. Nisida M, Saito H, A new interferometric method of two dimensional stress analysis, *Exp Mech*, 4(1964)366-376.
19. Fourney M E, Application of holography to photoelasticity, *Exp Mech*, 8(1968)33-38.
20. Hovanesian J D, Brcic J D, Powell R L, A new stress-optic method :stress-holointerferometry, *Exp Mech*, 8(1968)362-368.
21. Fourney M E, Mate K V, Further applications of holograph to photoelasticity, *Exp Mech*, 10(1970)177-186.
22. Holloway D C, Johnson R H, Advancements in holographic photoelasticity, *Exp Mech*, 11(1971)57-63.
23. Kubo H, Nagata R, Holographic photoelasticity with depolarized object wave, *Jpn J Appl Phys*, 15(1976)641-644.
24. Uozato H, Nagata R, Holographic photoelasticity by using dual hologram method, *Jpn J Appl Phys*, 16(1977)95-100.
25. Narayanamurthy C S, Dainty J C, Real-time holographic photoelasticity using BSO, *Opt Commun*, 91(1992)23-28.
26. Hecht E, Optics, 2nd edn, (Reading M A: Addision-Wesley), Chapter 8, 1987.
27. Jenkins F A, White H E, Fundamentals of Optics, 4th edn, (Auckland: McGraw-Hill International Book Co), Chapter 32, 1982.

28. Anand A, Narayanamurthy C S, Faraday rotation measurement with photorefractive $Bi_{12}TiO_{20}$, *Opt Laser Techno*, 34(2002)605-611.

[*Received*: 09.11.2019; *Revised*: 01.12.2019; *accepted*: 15.12.2019]

Appendix I

Consider Fig 2 in which both object beam and reference beam interfere inside a photorefractive crystal and can be represented as,

$$E_{opt}(r,t) = [E_1(z)\exp\{i(\vec{k_1}\cdot\vec{r} - \omega t)\} + E_2(z)\exp\{i(\vec{k_2}\cdot\vec{r} - \omega t)\}] + c\cdot c \quad \text{A.1}$$

Assuming that both object beam and reference beam amplitudes are slowly varying along z, the intensity distribution of light within the crystal can be expressed as,

$$I_t = [I_0 + (I_1 e^{ik_g x} + c\cdot c)] \quad \text{A.2}$$

where,

$$I_0 = \frac{n_0 c}{2\pi}\left(|E_1|^2 + |E_2|^2\right)$$

$$I_1 = \frac{n_0 c}{2\pi}\left(E_1 E_2^*\right)(\hat{n}_1\cdot\hat{n}_2)$$

And $\vec{k}_g = k_g\hat{x} = \vec{k_1} - \vec{k_2}$

In Eq (2), the normal vectors $\hat{n}_1$, $\hat{n}_2$ represent unit polarization unit vectors of object and reference beams, respectively and they are linearly polarized. The term k_g is grating vector. The intensity equation is also can be written as,

$$I_t = I_0[1 + M\cos(k_g x + \varphi)] \quad \text{A.3}$$

where, $M = 2(|I_1|/I_0)$ is modulation index and $\phi = \tan^{-1}(\text{Im } I_1/\text{Re } I_1)$.